

# Chemical mapping using reflection terahertz pulsed imaging

Y C Shen, P F Taday, D A Newnham and M Pepper

TeraView Limited, Platinum Building, St John's Innovation Park, Cambridge CB4 0WS, UK

E-mail: Yaochun.shen@teraview.com

Received 30 March 2005

Published 8 June 2005

Online at [stacks.iop.org/SST/20/S254](http://stacks.iop.org/SST/20/S254)

## Abstract

In this paper, we present the latest chemical mapping images of heterogeneous mixtures based on far-infrared reflection spectra obtained using a terahertz pulsed imaging system. The terahertz images and spectral data obtained have a spectral resolution of  $1\text{ cm}^{-1}$  and cover a spectral range of  $5\text{--}80\text{ cm}^{-1}$ . This broad spectral coverage enables us to map out the spatial distribution of individual chemical components of a sample in a single measurement.

(Some figures in this article are in colour only in the electronic version)

## 1. Introduction

Chemical mapping is an exciting new analytical advance that provides comprehensive information characterizing complex heterogeneous samples. The basis of chemical mapping is the acquisition of a three-dimensional data set where two axes describe vertical and horizontal spatial dimensions, and the third axis represents the spectral frequency dimension. In the near- and mid-infrared frequency range, Fourier-transform infrared (FTIR) and Raman spectroscopy have been successfully developed for chemical mapping [1–3]. In the far-infrared, however, the poor performance of conventional sources and detectors has made it impractical to develop an FTIR system for chemical mapping.

The newly developed technique of terahertz pulsed spectroscopy (TPS) has been demonstrated to have much better performance than FTIR systems in this low-frequency range [4–6]. A major advantage of TPS is that the transient electric field, not simply the intensity of the terahertz radiation, is measured. This coherent detection scheme not only yields terahertz spectra with excellent signal-to-noise ratio and high dynamic range, but also allows both absorption coefficients and refractive indices to be obtained without the need to apply the Kramers–Kronig dispersion relationship. Owing to these advantages, the terahertz pulsed technique has been investigated for both spectroscopic and imaging applications [7–14]. In particular, the capabilities of terahertz pulsed imaging (TPI) have been demonstrated in the clinical imaging of basal-cell skin carcinoma *ex vivo* and *in vivo* [15], and in the detection of hidden objects [16].

Very recently, a terahertz transmission imaging system based on a terahertz-wave parameter oscillator has been used for spectroscopic discrimination of illicit drugs [17]. For some practical applications such as security screening, terahertz measurements in reflection are highly desirable. Here we present the first chemical mapping images of heterogeneous mixtures based on far-infrared *reflection* spectra obtained using TPI.

## 2. Materials and method

Alpha-lactose monohydrate (Sigma-Aldrich, UK) and sucrose were studied. The lactose was milled to a fine powder (particle size  $<100\text{ }\mu\text{m}$ ). The sucrose was used in the original granulated form (particle size  $\sim 500\text{ }\mu\text{m}$ ). Lactose powder and sucrose were compressed under 2 tons using a hydraulic press (Specac, UK) to form circular pellets together with high-density polyethylene (PE, particle size  $<80\text{ }\mu\text{m}$ , Chesham Chemicals, UK). The PE powder acts as a pellet binder. Three pellets were prepared namely pure lactose, pure sucrose and a mixture of lactose and sucrose. These three pellets were mounted at the terahertz focus position for reflection measurements. Figure 1(a) shows a photograph of the samples used in the experiment.

A TPI<sup>TM</sup> scan imaging system (TeraView Ltd, Cambridge, UK), operating at a rapid scan mode (20 pixels per second) [17], was used in all measurements. In the experiment, the terahertz radiation reflected from a sample was measured in time domain over a scan range of about 5 mm, providing a spectral resolution of  $1\text{ cm}^{-1}$  in spectral range  $5\text{--}80\text{ cm}^{-1}$ .

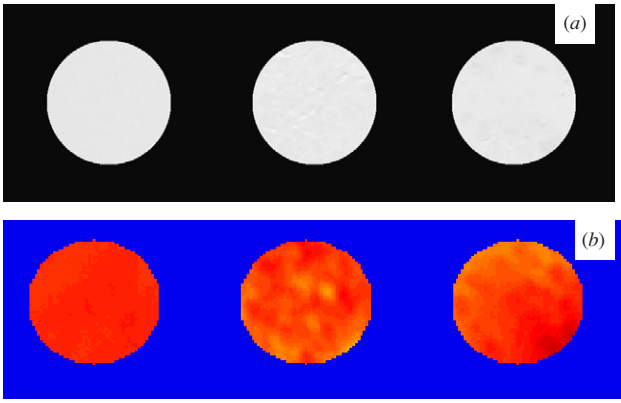


**Figure 1.** (a) Photograph of the pellet samples and (b) corresponding time-domain terahertz images. Left: lactose pellet; middle: sucrose pellet; right: lactose/sucrose mixture pellet.

Terahertz spectral images were obtained by raster scanning the terahertz beam across the sample. The scanning area is  $8 \text{ mm} \times 24 \text{ mm}$ , which corresponds to  $80 \times 240$  pixels at  $100 \mu\text{m}$  spacing. We note that the measurement time could be further reduced by using a fast single-shot technique [18] at the expense of signal-to-noise ratio and temporal resolution.

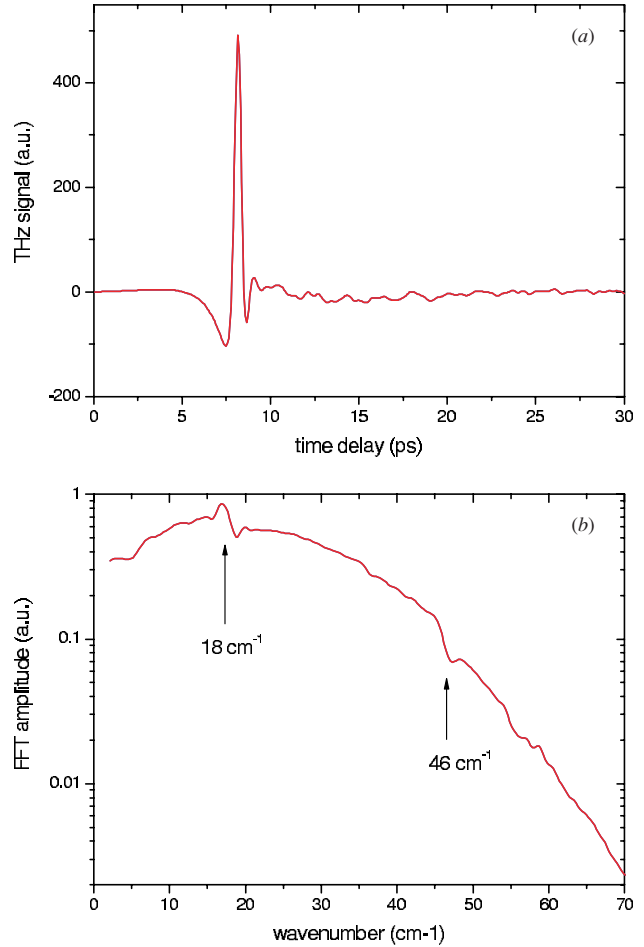
### 3. Results and discussions

Figure 1(b) shows an example time-domain terahertz image, which is produced by using the peak intensity of the temporal terahertz waveform at each pixel, with figure 2(a) showing a typical terahertz waveform. The main pulse of the terahertz waveform represents the terahertz reflection at the sample surface, and thus the peak amplitude of the main pulse is determined mainly by the change in refractive index at the air/sample interface. By comparing figures 1(a) and (b), one can see that even without any signal processing, the terahertz image already shows more detail of the sample than the photograph. The contrast in the terahertz images (as shown in the middle and right pellets of figure 1(b)) is interpreted as the refractive index variations in the pellets caused by large sucrose crystals and by the pellet compression process.

Figure 2(b) shows the Fourier transform of the measured terahertz waveform reflected from the centre of the pure lactose pellet. The absorption features of this form of lactose at  $18 \text{ cm}^{-1}$  and  $46 \text{ cm}^{-1}$  are clearly visible. The absorption coefficient,  $\alpha(\nu)$ , and the refractive index,  $n(\nu)$ , in the spectral range  $5\text{--}80 \text{ cm}^{-1}$  are then calculated for each pixel as

$$\sqrt{\varepsilon} \equiv n(\nu) + j \frac{\alpha(\nu)}{4\pi\nu} = \frac{1 - E_S(\nu)/E_M(\nu)}{1 + E_S(\nu)/E_M(\nu)}$$

where  $E_S(\nu)$  and  $E_M(\nu)$  are the Fourier transforms of the measured terahertz waveform reflected from a sample and a reference mirror. Figure 3 shows the first derivatives of the absorption coefficient of lactose and sucrose pellets. As expected, the first derivative spectra measured in reflection mode (curves labelled '1' in figure 3) are the same as those measured in typical transmission measurements (curves labelled '2' in figure 3). Therefore we can use terahertz transmission spectra, which are now available for a wide



**Figure 2.** A typical terahertz waveform recorded at the centre of lactose pellet (a), and the amplitude of its corresponding Fourier transform (b).

variety of chemicals, instead of terahertz reflection spectrum, as the basis for further chemical mapping processing.

Now we have obtained a three-dimensional data set where two axes describe vertical and horizontal spatial dimensions, and the third axis represents the spectral frequency dimension. In order to extract the spatial distributions of individual chemical substances in the sample, we first compress the three-dimensional data set to a two-dimensional matrix  $F_{N \times L}$ , which has  $L$  pixels each with  $N$  frequency components. If we assume that the sample has  $M$  chemical substances ( $M = 2$  for the present case) and each chemical substance has a known absorption spectrum with  $N$  frequency components, we then have a matrix of  $S_{N \times M}$ . The spatial distribution of individual chemical substances in the sample is then calculated using component analysis method as [16]

$$[P_{M \times L}] = ([S_{N \times M}]^T [S_{N \times M}])^{-1} [S_{N \times M}]^T [F_{N \times L}]$$

where  $P_{ij}$  represents the probability of the occurrence of the  $i$ th substance ( $i = 1$  for lactose, and  $i = 2$  for sucrose) at the  $j$ th pixel ( $j = 1, 2, \dots, L$ , and  $L = 80 \times 240$ ). Note that the spectral matrix  $S_{N \times M}$ , which forms the basis for chemical mapping analysis, can be obtained from either reflection or transmission terahertz measurements.

Figure 4(a) shows the terahertz image constructed using  $P_{ij}$  ( $j = 1, 2, \dots, L$ ), corresponding to spatial distribution of

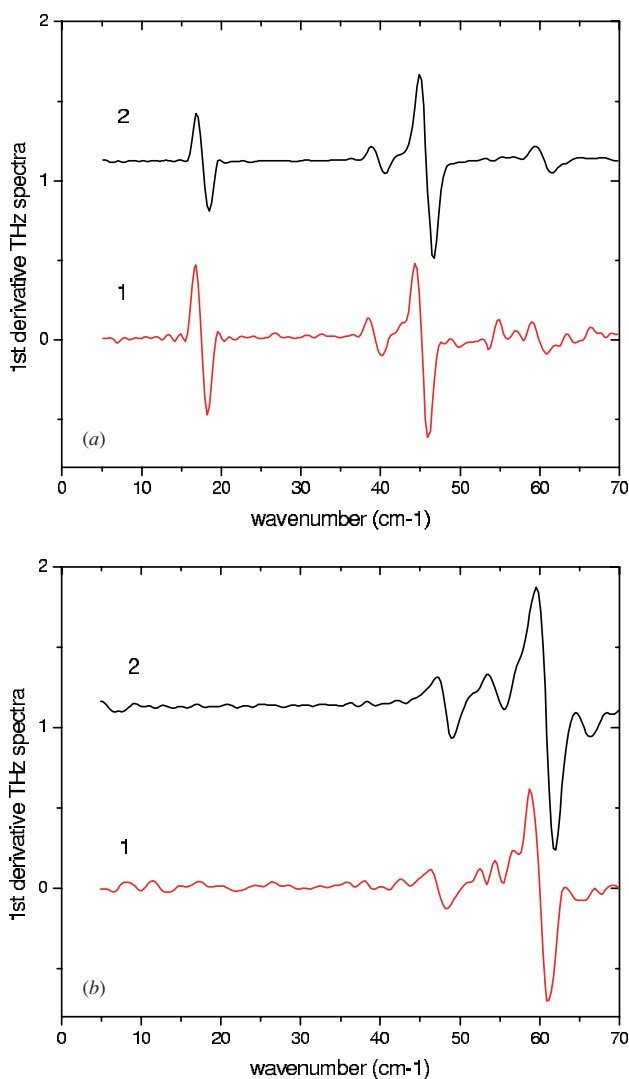


**Figure 3.** The first derivative spectra of the absorption coefficient of lactose (a) and sucrose (b). Curve 1: spectrum derived from terahertz reflection measurement; curve 2: spectrum derived from terahertz transmission measurement.

lactose. As expected,  $P_{1j}$  has large values across the entire lactose pellet (left of figure 4(a)), whilst  $P_{1j}$  is close to zero across most of the sucrose pellet (middle of figure 4(a)). The reverse is also true for the terahertz image shown in figure 4(b), which is constructed using  $P_{2j}$  ( $j = 1, 2, \dots, L$ ) and thus corresponds to spatial distribution of sucrose. It is interesting to note that the sucrose crystal particles are clearly visible in the terahertz image (figure 4(b)) whereas they cannot be identified in the photograph (figure 1(a)).

For the purpose of chemical mapping visualization, we set the  $j$ th pixel as lactose if  $P_{1j} > 0.4$ , sucrose if  $P_{2j} > 0.4$  and a mixture of lactose and sucrose where both  $P_{1j}$  and  $P_{2j}$  are greater than 0.4, i.e., where absorption features of both lactose and sucrose are found. In the false-colour image of figure 4(c), the lactose pixels are red, sucrose is blue and the lactose/sucrose mixture is pink. The green area represents an area where neither lactose nor sucrose absorption features were found, indicating pure polyethylene or the sample holder. These results have important implications for

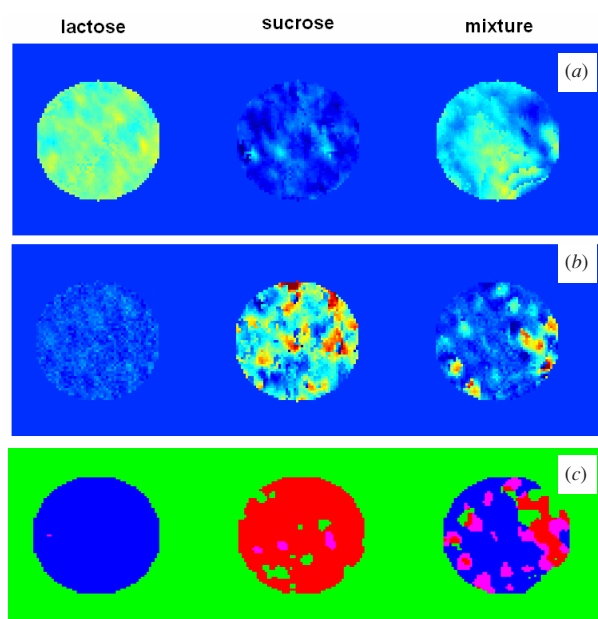


**Figure 4.** False-colour terahertz chemical mapping image showing the spatial distributions of (a) lactose, (b) sucrose and (c) reconstructed chemical map of the sample where blue shows lactose, red—sucrose, pink—both lactose and sucrose and green—neither lactose nor sucrose.

the quick detection and identification of chemical substances of special interest including drugs and explosives. For example, the presence and the shape of a piece of RBX-based plastic explosive have been recently detected and identified from our TPI reflection measurements, by using its spectral signatures in the range 5–50  $\text{cm}^{-1}$  [19].

We note that Watanabe *et al* [16] first demonstrated the non-destructive terahertz mapping of illicit drugs using spectral fingerprints at seven frequencies. Here we have further demonstrated that TPI can not only be used for detection and identification of different chemical pellets, but can also be used for chemical mapping the spatial distribution of individual chemical components in a heterogeneous mixture. Moreover, the TPI system used in our experiments has a continuous spectral coverage from 5 to 80  $\text{cm}^{-1}$ . This broad spectral range can be used to map out precisely the spatial distribution of an individual chemical substance in a multi-chemical sample with a single measurement. Furthermore, although the terahertz transmission imaging system has the advantage of quantitative analysis, a TPI system operating at reflection mode might be a better choice for a number of practical applications. For example, in this experiment, we used both fine lactose power and large sucrose particle samples with an average size of approximately 0.5 mm. Our transmission terahertz spectral measurements (not shown here) show that sucrose particles of this size are actually ‘opaque’ to terahertz radiation and therefore terahertz transmission imaging is no longer a proper tool for studying these samples. In contrast, as demonstrated here, a TPI system operating at reflection mode has no such limitation and can still be used to obtain reliable terahertz spectra for these large absorbing particles.

Finally we want to point out that the TPS system measures the transient electric field in the time domain, not simply the

intensity of the terahertz radiation. Therefore, both amplitude and phase of the THz pulse are obtained, and as a result, THz radiation reflected from different depths will arrive at different times. The combination of this THz time-of-flight tomography capability [20] and the chemical mapping capability as demonstrated here provides a TPI system with unique features of three-dimensional chemical mapping. Therefore TPI systems can map out the chemical distribution not only in the  $x$ - and  $y$ -directions (surface mapping), but also in the depth direction (3D volume mapping).

#### 4. Conclusions

In this paper, we have demonstrated the capability of TPI for detection and identification of different chemical materials and for chemical mapping the spatial distribution of individual chemical components in a heterogeneous mixture. The TPI images reported here cover a broad spectral range of 5–80  $\text{cm}^{-1}$  enabling us to map out precisely the spatial distribution of an individual chemical substance of a multi-chemicals sample in a single measurement.

#### References

- [1] Lewis E N, Treado P J, Reeder R C, Story G M, Dowrey A E, Marcott C and Levin I W 1995 *Anal. Chem.* **67** 337
- [2] Koenig J L, Wang S Q and Bhargava R 2001 *Anal. Chem.* **A 73** 360
- [3] Clarke F C, Jamieson M J, Clark D A, Hammond S V, Jee R D and Moffat A C 2001 *Anal. Chem.* **73** 2213
- [4] Dorney T D, Baraniuk R G and Mittleman D M 2001 *J. Opt. Soc. Am. A* **18** 1562
- [5] Ferguson B and Zhang X-C 2002 *Nature Mater.* **1** 26
- [6] Beard M C, Turner G M and Schmuttenmaer C A 2002 *J. Phys. Chem. B* **106** 7146
- [7] Walther M, Fischer B, Schall M, Helm H and Uhd Jepsen P 2000 *Chem. Phys. Lett.* **332** 389
- [8] Shen Y C, Upadhy P C, Davies A G and Linfield E H 2003 *Appl. Phys. Lett.* **82** 2350
- [9] Taday P F, Bradley I V, Arnone D D and Pepper M 2003 *J. Pharm. Sci.* **92** 831  
Strachan C J, Rades T, Newnham D A, Gordon K C, Pepper M and Taday P F 2004 *Chem. Phys. Lett.* **390** 20  
Fitzgerald A J, Cole B E and Taday P F 2005 *J. Pharm. Sci.* **94** 177
- [10] Walther M, Fischer B M and Uhd Jepsen P 2003 *Chem. Phys.* **288** 261
- [11] Hu B B and Nuss M C 1995 *Opt. Lett.* **20** 1716
- [12] Mittleman D M, Gupta M, Neelamani R, Baraniuk R G, Rudd J V and Kock M 1999 *Appl. Phys. B* **68** 1085
- [13] Ferguson B, Wang S H, Gray D, Abbott D and Zhang X C 2002 *Phys. Med. Biol.* **47** 3735
- [14] Shen Y C, Upadhy P C, Linfield E H and Davies A G 2004 *Vib. Spectrosc.* **35** 111
- [15] Wallace V P, Fitzgerald A J, Shankar S, Flanagan N, Pye R J, Cluff J and Arnone D D 2004 *Br. J. Dermatol.* **151** 424
- [16] Watanabe Y, Kawase K, Ikari T, Ito H, Ishikawa Y and Minamide H 2003 *Appl. Phys. Lett.* **83** 800
- [17] Kemp M C, Taday P F, Cole B E, Cluff J A, Fitzgerald A J and Tribe W R 2003 *Proc. SPIE* **5070** 44
- [18] Ferguson B, Wang S, Gray D, Abbott D and Zhang X C 2002 *Microelectron. J.* **33** 1043
- [19] Shen Y C, Newnham D A, Taday P F and Kemp M C 2005 Presented at *Photonic West 2005 (San Jose, California, 22–27 Jan. 2005)*
- [20] Zhang X C 2004 *Phil. Trans. R. Soc. A* **362** 283